

THE EFFECT OF ENVIRONMENT ON THE FORMATION OF H α FILAMENTS AND COOL CORES IN GALAXY GROUPS AND CLUSTERS

MICHAEL McDONALD^{1,2}, SYLVAIN VEILLEUX^{1,3} AND RICHARD MUSHOTZKY¹

Draft version August 23, 2021

ABSTRACT

We present the results of a combined X-ray and H α study of 10 galaxy groups and 17 galaxy clusters using the *Chandra X-ray Observatory* and the Maryland Magellan Tunable Filter. We find no difference in the morphology or detection frequency of H α filaments in groups versus clusters, over the mass range $10^{13} < M_{500} < 10^{15} M_{\odot}$. The detection frequency of H α emission is shown to be only weakly dependent on the total mass of the system, at the 52% confidence level. In contrast, we find that the presence of H α filaments is strongly correlated with both the global (89% confidence level) and core (84%) ICM entropy, as well as the X-ray cooling rate (72%). The H α filaments are therefore an excellent proxy for the cooling ICM. The H α filaments are more strongly correlated with the cooling properties of the ICM than with the radio properties of the BCG; this further supports the scenario where these filaments are directly associated with a thermally-unstable, rapidly cooling ICM, rather than radio bubbles. The ICM cooling efficiency, defined as the X-ray cooling rate per unit gas mass, is shown to correlate with the total system mass, indicating that groups are more efficient at cooling than clusters. This result implies that, in systems with cool cores, AGN feedback scales with the total mass of the system, in agreement with earlier suggestions.

Subject headings: galaxies: cooling flows – galaxies: clusters – galaxies: groups – galaxies: elliptical and lenticular, cD – galaxies: active – ISM: jets and outflows

1. INTRODUCTION

The high X-ray surface brightness in the cores of some galaxy clusters suggests that, in the absence of any feedback, radiative cooling should become a runaway process, leading to “cooling flows” of 10–100 $M_{\odot} \text{ yr}^{-1}$ (see review by Fabian 1994). A distinguishing characteristic of cool core clusters is the presence of warm, optical line-emitting gas (Hu et al. 1985, Heckman et al. 1989, Crawford et al. 1999, Jaffe et al. 2005, Hatch et al. 2007). Typically observed at H α , this warm gas generally exhibits either a nuclear or filamentary morphology and has been shown to correlate with several properties of the cool core, such as cooling rate and cluster entropy (McDonald et al. 2010; hereafter M+10). Despite the near ubiquity of optical line-emitting nebulae in cool core clusters, their origins remain unclear. In M+10 we considered several processes for producing the observed H α morphology, and found that the observations were consistent with two formation scenarios: 1) the warm gas cooled out of the X-ray, and 2) the warm gas was entrained behind buoyant radio bubbles arising from AGN feedback (e.g. Churazov et al. 2001, Reynolds et al. 2005, Vernaleo et al. 2007, Revas et al. 2008). The high H α surface brightnesses measured in these systems indicate that additional ionization sources are present, allowing the ionized gas to recombine more than once. Crawford et al. (2005) describe potential sources of ionization, the most promising of which are: 1) cosmic ray ionization, 2) heat conduction from the ICM to the colder filaments, and 3) photoionization by hot young stars. In McDonald et al. (2009) and M+10 we provide evidence for both star

formation and conduction, respectively, but were unable to rule in favor of a dominant ionization mechanism.

While much effort has gone into quantifying and explaining the presence of warm filaments in clusters, very little work has been done on the environmental dependence of this phenomenon. While massive clusters of galaxies are dominated by gravitational and thermal processes, their low-mass counterparts, galaxy groups, may be dominated by non-gravitational processes such as winds, cooling flows or AGN feedback (Sun et al. 2009a). Thus, by considering low-mass systems we can hope to find out whether the observed phenomena are more closely related to global, gravitational processes or more local, baryon physics. In M+10, we showed that the properties of the H α filaments were strongly correlated with the properties of the cluster core, such as the cooling rate, cooling radius, entropy and temperature. However, most of these trends only cover a small range in X-ray properties, since M+10 only considered clusters.

In an effort to properly evaluate the dependence of the H α filaments on environment, we have conducted a survey of 10 galaxy groups using the Maryland Magellan tunable filter (hereafter MMTF; Veilleux et al. 2010). We combine this sample of 10 groups with a subset of 17 clusters drawn from M+10. In §2, we describe this sample in more detail, along with the data acquisition and analysis. In §3, we present the results of this study, re-examining several trends found by M+10, and also exploring new issues. In §4 we discuss the implications of these results and postulate on the origin and power source of these warm filaments. Finally, in §5 we conclude and discuss prospects for future studies.

Throughout this paper, we assume the following cosmological values: $H_0 = 73 \text{ km s}^{-1} \text{ Mpc}^{-1}$, $\Omega_{\text{matter}} = 0.27$, $\Omega_{\text{vacuum}} = 0.73$.

¹ Department of Astronomy, University of Maryland, College Park, MD 20742

² Email: mcdonald@astro.umd.edu

³ Email: veilleux@astro.umd.edu

2. DATA COLLECTION AND ANALYSIS

2.1. Sample Selection

The goal of this study is to extend our investigation of H α filaments (M+10) from the cluster to group environment. Thus, we begin with a sample drawn from M+10, of 17 cool core clusters. These clusters were originally chosen from the larger sample of White et al. (1997). This large sample, much like any X-ray selected sample, is inherently biased towards cool cores due to their higher surface brightness. The full sample of 207 clusters (White et al. 1997) was reduced based on the following criteria: 1) visible with the Magellan telescope ($\delta < 35^\circ$); 2) appropriate redshift to be imaged at H α with MMTF ($0.0 \leq z \leq 0.09$). From this reduced sample, we choose 17 clusters with high-quality Chandra imaging, covering three orders of magnitude in classical cooling rate. These clusters were chosen to yield a relatively flat distribution of cooling rates, ensuring that we covered the full gamut of cool core and non cool core clusters. This selection technique will, of course, introduce a significant bias, the effects of which will be discussed later in §4. The 17 selected clusters all have deep H α imaging from MMTF, as presented in M+10.

From the sample of 43 galaxy groups defined by Sun et al. (2009a), we chose at random 10 groups which obey the same criteria as above, with average temperatures ranging from 0.7–3 keV, to add to this sample. Unlike the White et al. (1997) sample, this collection of 43 galaxy groups is not based solely on X-ray detections of clusters. Sun et al. (2009a) include AGN-selected and optically-selected groups, removing much of the bias towards cool cores that affects X-ray selected catalogs. Thus, the 10 groups in our sample should be relatively unbiased in mass, temperature and cooling rate.

The full sample is listed in Table 5. We discuss below the processing of the new MMTF H α observations and the archival Chandra X-ray data.

2.2. H α : MMTF

MMTF has a very narrow bandpass ($\sim 5\text{--}12\text{\AA}$) which can be tuned to any wavelength over $\sim 5000\text{--}9200\text{\AA}$ (Veilleux et al. 2010). Coupled with the exquisite image quality at Magellan and the wide field of the Inamori-Magellan Areal Camera & Spectrograph (IMACS), this instrument is ideal for detecting emission-line filaments in galaxy groups and clusters. In M+10 we presented deep MMTF H α observations of 23 clusters (17 of which have high-quality CXO data). As a follow-up to that project, we have observed an additional 10 groups during 2009-10 at both H α ($\lambda=6563\text{\AA}$) and continuum ($\pm 60\text{\AA}$), for a total of 40 minutes each with the largest available bandpass ($\sim 12\text{\AA}$). The typical image quality for these exposures was $0.6 \pm 0.2''$. These data are a significant improvement on previous narrow-band imaging of cluster cores due to the very narrow ($\sim 10\text{\AA}$) bandwidth of the MMTF. This allows us to isolate and measure the flux of the H α line without making any assumptions about the [N II]/H α ratio.

These new data were fully reduced in exactly the same way as the M+10 data, using the MMTF data reduction pipeline⁴, which performs bias subtraction, flat fielding,

sky line removal, cosmic ray removal, astrometric calibration and stacking of multiple exposures (following Veilleux et al. 2010; see also Jones, Bland-Hawthorn, Shopbell 2002). The continuum image was then PSF and intensity matched to the narrow-band images to allow for careful continuum subtraction. The stacked images were calibrated using spectrophotometric standards from Oke (1990) and Hamuy et al. (1992, 1994). The error associated with our absolute photometric calibrations is $\sim 15\%$, which is typical for tunable filters and spectrographs. Finally, the data were corrected for Galactic extinction, following Cardelli et al. (1989) using reddening estimates from Schlegel et al. (1998). We do not attempt to correct for intrinsic extinction since the dust content of the optical filaments is not well known. All of these procedures are described in detail in Veilleux et al. (2010).

For systems with complicated morphologies, H α fluxes were measured by creating (by eye) a region which generously traced the H α emission and calculating the total signal within this region. For more symmetric morphologies, a circular aperture centered on the emission peak was used, with the radius chosen to contain all of the obvious emission. We show in M+10 that this technique yields fluxes that agree relatively well with those in the literature.

2.3. X-Ray: Chandra

Archival data from the *Chandra X-ray Observatory* were retrieved for all 10 of our sample groups. In order to ensure a homogeneous treatment of the X-ray data, the clusters data were re-reduced alongside the groups data. These data were reprocessed with CIAO (version 4.1.2) and CALDB (version 4.1.1) using the latest time-dependent gain adjustments and maps to create new level 2 event files. Due to the large angular extent of some of the groups and clusters in our sample, we were required to construct blank-sky background event files, using the ACIS blank-sky background database, to properly account for background flux. The new level 2 event files were cleaned for flares, using the *lc_clean* routine, by examining the light-curve and removing any spurious bursts in intensity. These data cleaning and calibration procedures are all outlined in detail in the CIAO science threads⁵.

In order to separate the filaments or other substructures from the X-ray halo, we applied an unsharp mask to each image, subtracting a $10''$ Gaussian smoothed image from a $1.5''$ Gaussian smoothed image. The resulting image highlights any fine structure in the X-ray morphology (see Figure 1).

For each object, background-subtracted spectra were extracted using *dmextract*. Updated response files were created using *mkacisrmf* and *mkwarf*, following the CIAO science threads. Counts were grouped into bins with 20 counts per bin, over the range 0.3 to 11.0 keV. Spectra were extracted in a variety of regions to better understand the relationship between the ICM and the H α emission. These regions include: i) circular annuli, with spacing chosen so that $r_{out}/r_{in} = 1.25\text{--}1.6$ (following Sun et al. 2009a, McDonald et al. 2010), ii) Coincident with the H α -emitting filaments, and iii) the regions

⁴ <http://www.astro.umd.edu/~veilleux/mmtf/datared.html>

⁵ <http://cxc.harvard.edu/ciao/threads/>

surrounding, but not overlapping with, the H α -emitting filaments.

In order to derive physical quantities from the X-ray spectra, we used the XSPEC spectral fitting package (Arnaud 1996). For the circular annuli, we first deproject the data in each radial bin using the direct spectral deprojection method (DSDEPROJ; Russel et al. 2008). We then model the spectra with a combination of photoelectric absorption (PHABS) and thermal brehmsstrahlung emission from a hot diffuse gas (MEKAL). This combination of models has 3 free parameters which describe the state of the ICM: T_X , n_e , and Z . In order to measure the strength of the ICM cooling, we also allow for an additional component which represents gas cooling over a range of temperatures (MKCFLOW), which has an additional free parameter, dM/dt .

For a more complete description of the spectral extraction and modeling techniques, the reader is directed to McDonald et al. 2010.

3. RESULTS

3.1. Warm Ionized Filaments

The primary strengths of MMTF are its large field of view and excellent angular resolution. These make it ideally suited to search for thin, extended filaments in the cores of clusters, as we showed in M+10. Our previous study of galaxy clusters revealed a wide variety of filament morphologies, leading us to develop a classification scheme to help with the analysis of such a diverse sample. We found that 35% of clusters exhibited thin, extended H α filaments (type I), 30% had nuclear or only marginally extended H α emission (type II), and 35% had no detectable H α emission at all. We adopt this same nomenclature for our new sample of 10 galaxy groups, finding very similar ratios between the three types (30% : 30% : 40%). The similar frequency with which we detect H α filaments in groups compared to clusters suggests a similar formation mechanism.

In Figure 1 we show the new data for 10 galaxy groups. For all 10 groups in this sample we show the MMTF red continuum, smoothed CXO, unsharp masked CXO, and MMTF H α images. Just as we saw for clusters, the presence of complex morphology in the X-ray appears to correlate with the presence of H α filaments. We find that all three clusters with strongly asymmetric residuals in the unsharp masked X-ray images have extended H α filaments. We will investigate this relationship between the X-ray and H α data further in the following sections.

Of particular interest in Figure 1 is the morphology of the H α emission for Abell 1991 and NGC 4325 (Sersic 159-03 was discussed in M+10). Abell 1991 has an arrow-shaped morphology, extending north from the BCG nucleus. This morphology is reminiscent of a bowshock. We find that the arrow-head corresponds to a bright blob of soft X-rays, while the peak of H α emission at the base of the arrow has no X-ray counterpart. The second interesting group, NGC 4325, exhibits several distinct, radial filaments. This complex morphology strongly resembles the core of the Perseus cluster. Unlike Perseus, the central galaxy in NGC 4325 is almost completely isolated and the total X-ray mass is an order of magnitude lower. This suggests that the global properties of the group/cluster plays only a minor role in the

presence and morphology of H α emission.

3.2. Global and Core X-Ray Properties

In order to compare properties of groups and clusters, we adopt a scale radius at which we measure quantities such as temperature, density, entropy and enclosed mass. The radius we use, r_{2500} , is the radius at which the average enclosed density is 2500 times the critical density of the Universe. This radius is considerably smaller than the more commonly used value of r_{500} , however we prefer using r_{2500} due to our ability to directly measure quantities at r_{2500} (which we will refer to as ‘‘global’’ parameters), rather than infer them indirectly from other measurements. The typical value of r_{500} for the groups in our sample is ~ 600 kpc (Sun et al. 2009a), which corresponds to a diameter of $\sim 20'$ at a typical redshift of 0.05 – larger than the typical CXO field of view. Thus, we choose a smaller radius at which we can measure various properties for all of the groups and clusters in our sample.

In Figure 2 we plot various X-ray scaling relations for our full sample. For systems in hydrostatic equilibrium, we expect a direct correlation between the total enclosed mass and the gas temperature for a given radius, which we observe in general. However, we also find several systems which deviate from this relation. This is because clusters are often not fully in hydrostatic equilibrium due to processes such as AGN feedback or mergers. Nevertheless, these scaling relations show the broad range in parameters covered by the groups and clusters in this sample.

At a glance, Figure 2 offers no new insight into the presence of H α filaments. We detect H α in systems at all temperature, mass and entropy, with no obvious bias. To further quantify this, we consider both the fraction of systems with non-zero H α flux and those with extended H α filaments as a function of global X-ray properties in Figure 3. We have chosen the binning such that the number of systems in each bin are roughly equivalent. In each panel, we show the F-test likelihood that the histogram is flat, compared to monotonically increasing or decreasing. This statistic confirms that, at the 87% confidence level, the presence of H α emission is uncorrelated with the global temperature. Additionally, we find only a weak correlation between the presence of H α emission and system mass (52% confidence level).

We note that, in higher mass/temperature systems, the fraction of systems with H α emission is likely an upper limit, due to our bias towards cool cores in these systems. Thus, while there is only a weak correlation between the presence of H α emission and the global mass, the trend would likely be strengthened by the inclusion of high mass, non cool-core systems which we would not expect to emit at H α based on our previous work (M+10).

The bottom two panels of Figure 3 show the distribution of the entropy and the gas mass fraction for systems with non-zero H α flux or with extended H α filaments. We find a correlation between entropy and the presence of H α filaments (89% confidence level). We find that 12 of the 15 systems with $K < 900$ keV cm 2 show filaments, while only 5 of the 11 systems with $K > 900$ keV cm 2 show filaments. This is consistent with findings by previous studies (Cavagnolo et al. 2008, McDonald et al. 2010) which show that low-entropy systems tend

to have more star formation and optical line emission. Finally, we observe very few systems with H α filaments and very low X-ray gas mass fractions, suggesting that the two gas phases are related (51% confidence level). This seems to favor the hypothesis that the warm ionized gas is intimately linked to the hot gas – a certain threshold amount of hot gas is needed in order for H α filaments to exist. In summary, Figure 3 suggests that the presence of H α emission is only weakly dependent on the global mass (and thus, temperature) of the system. However, the state of the ICM (i.e. entropy, fractional gas mass) may help dictate whether these filaments can exist.

In M+10, we provided evidence that the observed H α filaments were intimately linked to the X-ray cooling. Thus, we re-examine the properties of the group/cluster cores, where the gas is cooling on a short timescale. Figure 4 provides similar histograms to those described above, but now considering only measurements taken in the group/cluster core. We calculate the frequency of H α emission as a function of the 1.4 GHz radio power, which traces AGN feedback, the X-ray cooling rate, the average temperature within the central 100 kpc, and the entropy at a radius of 50 kpc. We find a weak correlation between the 1.4 GHz luminosity and the presence of H α filaments (56% confidence level). In contrast, the correlation with the X-ray cooling rate is significantly stronger (72%), as we also found in M+10. This suggests that the ionized filaments are linked more closely to the cooling ICM than to the radio-loud AGN. In the lower panels, we see a much stronger dependence on temperature and entropy when we move to smaller radius. There appear to be very few systems with H α filaments and high temperature/entropy in the inner regions. This confirms our findings from M+10 that the presence of H α filaments correlates with the temperature (55% confidence level) and entropy (84% confidence level) inside of the cooling radius. The results of Figure 4 are not strongly affected by our selection biases. The missing clusters, which should be high-mass with no cool core, should have high entropy and temperature in the inner 100 kpc. Since we expect these non-cooling systems to lack H α emission, the trends would remain the same.

The combination of Figures 3–4 suggests that the presence of H α filaments is a function of the state of the ICM inside of $\sim r_{cool}$ and is largely independent of the global properties much beyond this.

3.3. X-Ray – H α Correlations

In M+10 we provided several pieces of evidence which link the observed H α filaments to the X-ray cooling. With the addition of 10 additional low-mass systems, it is relevant to return to these results and ensure that they are still significant.

In Figure 5 we plot both the total H α luminosity and the H α luminosity in filaments as a function of various X-ray properties of the cool core. In M+10 we found that systems with warm cores ($kT_{100} > 4.5$ keV) do not emit at H α , while systems with cool cores can have H α emission, but not always. This trend is preserved by including cooler systems (blue points). Additionally, we saw correlations between the H α luminosity in filaments and the X-ray cooling rate and core entropy values. These trends are strengthened by the addition of low-mass sys-

tems, which exactly follow the distribution of high-mass systems. The strong correlation between the H α luminosity and the X-ray cooling rate suggests a direct link between the cooling ICM and the warm gas.

In addition to a correlation between the mass of gas cooling below the hot phase and the mass of warm gas, we also found, in M+10, a correlation between the extent of the warm gas and the cluster cooling radius. The addition of 10 additional groups to this result (Figure 6) further strengthens our claim that the size of the H α filaments do not exceed the cluster cooling radius. Since the location of the cooling radius is dependent on an arbitrarily-assigned cooling time, we have tested cooling times of both 3Gyr and 5Gyr. While M+10 showed that a cooling radius based on $t_{cool} = 5$ Gyr matched the data well, we show in Figure 6 that $t_{cool} = 3$ Gyr does a significantly better job of defining the maximum radius of H α emission. The fact that we do not see H α emission beyond the radius at which the hot ICM is cooling in less than 3Gyr suggests a natural timescale for the formation of these filaments.

In §2.2, we discussed the procedure of extracting X-ray spectra coincident to and surrounding the observed H α filaments. Since we are unable to determine the 3-dimensional shape of these filaments, we attempt to model them using two different geometries: 1) thick slabs of gas extending into the sky for the full length of the cluster, modeled with a single-temperature plasma, and 2) thin, cylindrical filaments that are modeled with a two-temperature plasma to account for the background/foreground gas seen in projection. In Figure 7, we show the results of this exercise for the groups and clusters in our sample which exhibit extended filaments. As we found in M+10, the X-ray gas coincident with the H α filaments (labeled “in”) appears to be cooling faster than the surrounding ICM (labeled “out”). Assuming thin-filament geometry, the X-ray temperature of the filaments is ~ 20 –50% that of the off-filament gas at the same radius for most of the systems. Additionally, both the entropy and cooling time of the filaments is roughly an order of magnitude smaller for gas in the filaments than off-filament gas at similar radii. Even if we assume that the “filaments” are sheets seen in projection, we infer a cooling time half as long for in-filament gas. We find no significant difference in the filament properties between groups and clusters, suggesting that they share the same formation mechanism.

Figure 7 offers unique evidence for a link between the hot and warm gas phases. The fact that the hot gas is cooling an order of magnitude faster in the filaments provides a direct connection between the X-ray cooling flow and the H α filaments. Coupled with the correlation between the cooling rate and H α flux contained in filaments, the evidence for a link between the H α filaments and the X-ray cooling flow is further strengthened. The fact that we see no obvious differences between the properties of the filaments in groups and clusters suggests that the formation mechanisms for these filaments are the same. We discussed formation scenarios in depth in M+10, but the addition of the lower mass systems now provide new insights in the discussion (next section).

4. DISCUSSION

4.1. Groups vs Clusters: Differences and Similarities

Despite the smooth transition in mass and temperature from groups to clusters, the former are not simply scaled down versions of the latter. We summarize the most relevant differences between the two below.

- Feedback processes such as radio jets, starburst-driven winds, and merging with other bound systems will dominate in the group environment, while they play second fiddle to gravitational processes in the cluster environment. At $M \lesssim 10^{14} M_{\odot}$ the total radio heating energy of the BCG AGN (assuming $\epsilon = 0.1$; Sun et al. 2009b) becomes larger than the total potential or thermal energy of the ICM.
- While clusters form at late cosmological times ($z \lesssim 1$), groups have been forming over almost the entire age of the universe ($z \lesssim 10$; Fakhouri et al. 2010). Since age roughly correlates with several X-ray observables (entropy, gas fraction) one would expect groups to have a much broader range of properties due to their substantial spread in ages.
- In galaxy clusters, the ratio of the total mass in gas to dark matter is roughly 1:10, with a negligible contribution from light in stars using standard mass-to-light ratios. However, in galaxy groups, the stellar mass fraction is an order of magnitude higher, leading to significantly lower mass to light ratios (Giodini et al. 2009). Additionally, the gas fraction decreases as a function of total mass, such that groups can have stellar to dark matter ratios of roughly 1:10, with a negligible contribution from the ICM. Clearly this limits the influence that the ICM can have on the rest of the system.

Remarkably, although there are such vast differences between clusters and groups, we find very little dependence of $H\alpha$ emission on the global mass or temperature of the group/cluster. The fact that we see similar cooling rates and optical line flux in systems with orders of magnitude less gas implies that groups are more efficient in their cooling. In order to pursue this notion, we consider the cooling properties of the group/cluster as a function of the system mass (M_{2500}). In Figure 8 we first show the X-ray mass deposition rate, dM/dt , as a function of the group/cluster mass, M_{2500} . In order to improve the mass coverage, we have added 6 additional groups from the Sun et al. (2009a) sample – these systems do not have $H\alpha$ imaging. We observe a steady increase of the cooling rate as a function of total mass, which is not surprising since there is more gas available for cooling. In order to remove this dependence on system mass, we next consider the amount of gas cooling out of the X-ray, per solar mass of material in the group/cluster (upper right panel of Figure 8). We see no observable trend between these two quantities. However, we do detect what looks like an upper limit to the cooling rate per unit mass, such that the maximum cooling is $\sim 0.02\%$ of the cluster mass per Gyr.

If, instead, we consider the *ICM cooling efficiency*, defined as the amount of gas cooling out of the X-ray per solar mass of *gas* in the group/cluster, we see a correlation (Pearson $R=0.71$). We can understand this correlation

by considering the following: (1) The presence of cool cores is only weakly dependent on mass (Figure 3); (2) The total amount of gas is strongly dependent on mass. Combining these two points naturally leads to a correlation between the ICM cooling efficiency and the system mass. Similarly, we can show the same trend using the $H\alpha$ -derived star formation rate (directly proportional to $L_{H\alpha}$), instead of the X-ray cooling rate, since these two quantities are strongly correlated. As we discussed in §2, this sample is biased against massive, non-cool core clusters. We point out that the correction of this bias would introduce additional high-mass, low effective cooling rate points to Figure 8. As with Figure 3, this correction would act to strengthen the observed correlation. This correlation suggests that groups are more efficient at cooling than clusters, despite the fact that feedback processes dominate in this region.

To better understand this trend, we can approximate the expected relationship of the ICM cooling efficiency with total mass:

$$\left(\frac{dM}{dt} \frac{1}{M_G}\right) \sim \left(\frac{M_G}{t_{cool} M_G}\right) \sim \frac{1}{t_{cool}} \sim \left(\frac{kT}{n\Lambda}\right)^{-1} \propto \frac{\Lambda}{kT} \quad (1)$$

$$\Lambda \propto \left\{ \begin{array}{ll} T^{1/2} & (T > 4 \times 10^7 \text{ K, Bremsstrahlung}) \\ T^{-0.6} & (T < 4 \times 10^7 \text{ K, Line cooling}) \end{array} \right\} \quad (2)$$

Equation 1 makes the assumption that the local ICM density is roughly independent of the temperature, which we have confirmed for the groups/clusters in our sample. If we couple equations 1 and 2 with the relation between M and T found by Sun et al. (2009a; $M \propto T^{1.7}$), we find the dependence of the ICM cooling efficiency on mass matches well with the observations (see Figure 8). While this derivation is overly simplistic, the confirmation with observation is reassuring. A major issue with such a simple derivation is that it ignores the role of feedback. In low-mass systems, one would expect the relative energy contribution from the AGN to increase substantially, yielding *less* efficient cooling. The fact that we observe the opposite suggests two possible scenarios for cool core clusters: i) AGN feedback plays a negligible role in countering ICM cooling, or ii) AGN feedback scales with environment. The former explanation is in opposition to a rich literature on the subject, both theoretical (e.g., Brighenti et al. 2003; Croton et al. 2006; Cattaneo et al. 2007; McCarthy et al. 2010) and observational (e.g., Bîrzan et al. 2004; Donahue et al. 2006; Rafferty et al. 2008; Sun 2009b), which offers significant evidence for AGN feedback playing a dominant role in the heating of galaxy group/cluster cores. The second explanation, that AGN feedback scales with environment, is more plausible. This scenario was recently investigated by Sun (2009b), who found that, in cool core groups and clusters, the radio luminosity of the central AGN scales with the cooling luminosity. Sun found that cool cores in groups have consistently lower 1.4 GHz luminosity AGN than in clusters and suggested that the lower-pressure intragroup medium may not be able to sustain the radio-loud AGN seen in the cores of massive clusters. We elaborate on this idea in Figure 9.

Motivated by Figure 1 from Sun (2009b), Figure 9 shows the 1.4 GHz luminosity ($L_{1.4GHz}$) as a function of the soft X-ray luminosity ($L_{0.5-2keV}$) inside of the cooling radius ($L_{0.5-2keV}$). We show in light grey points the distribution of groups and clusters from Sun (2009b), while the red ellipses show the loci of these distributions. Sun identified two classes of system: coronae, which show no correlation between the cool X-ray and radio luminosities, and luminous cool cores, which have cool X-ray luminosity correlated with radio luminosity. We show in Figure 9 our proposed, simplified evolution of these systems. Luminous cool cores are experiencing feedback-regulated cooling, such that both the AGN and cool core are able to grow slowly over timescales on the order of Gyr, based on measured cooling times in the central 100kpc. However, once the radio luminosity of the AGN reaches a certain threshold, it has enough energy to equal the PdV work required to evacuate the cool gas from the central 10kpc – this threshold radio luminosity is depicted by a dotted horizontal line for three different mass regimes. Thus, systems experiencing sufficiently strong radio-mode feedback have disrupted cool cores where the radio and X-ray luminosities are decoupled, yielding a corona-class object. Given the relatively few objects occupying the space between corona and cool core systems, the disruption of the cool cores must happen relatively quickly (\ll Gyr). With no cooling flow to fuel the central AGN, the radio luminosity will eventually drop until cooling is allowed again. Assuming the cool core is fully disrupted, it should take a few Gyr for gas which was originally at the cooling radius to form a new cool core. At this point, the central black hole becomes active once more and the feedback loop is re-established.

In Figure 9 there are three systems with radio luminosities sufficiently higher than the threshold for their mass – Hydra A, Abell 2052, and Abell 4059. These systems are all known to be experiencing higher-than-normal radio-mode feedback and have severely disrupted cool cores (e.g. Wise et al. 2007; Reynolds et al. 2008; Blanton et al. 2009). These systems all lie slightly off of the locus of points for luminous cool cores, suggesting that they may be in the midst of evolving from cool core to corona class via a disruption of the cool core.

In summary, Figures. 8–9 tell an interesting story about the cool cores of groups and clusters. The evidence suggests that groups are more efficiently converting the hot ICM into cool gas, as we detect H α filaments and cool cores with similar luminosity in systems with orders of magnitude difference in gas mass. It is unsurprising that groups are cooling more efficiently, since the majority of the intragroup gas is already at low temperature. However, the fact that this cooling is allowed to proceed as expected suggests that AGN feedback, which we assume regulates the cooling process, scales with system mass as well. We confirm the findings by Sun (2009b) that this is indeed the case, with cool cores in groups harboring radio-quiet AGN, while cool cores in massive clusters tend to have radio-loud AGN. This scaling of feedback strength with environment is a result of cool cores in low mass systems being more easily disrupted than those in high-mass systems.

4.2. The Origin of H α Filaments in Groups and Clusters

As discussed in M+10, we find strong evidence for a link between the cool core and the observed H α filaments. Summarized briefly, the main pieces of evidence in favor of this scenario are:

1. The soft X-ray and H α morphologies are correlated (Figure 1)
2. There is a correlation between the H α luminosity and the X-ray cooling rate (Figure 5)
3. H α filaments extend all the way to the X-ray cooling radius, but never beyond (Figure 6).
4. The ICM coincident with the H α filaments is cooling an order of magnitude faster than in the immediately surrounding regions (Figure 7).

We find that all of these trends, originally quoted in M+10, are seen in groups as well. This argues strongly in favor of a common origin and suggests that the cooling process may be detached from the global properties of the system.

The link between the X-ray cooling properties and the optical emission suggests that the H α filaments trace the cooling flow. This is not to say that the H α emission is due to the cooling ICM recombining at 10^4 K, but rather that the morphology of the H α filaments is reminiscent of magnetohydrodynamic simulations of gas cooling. As the ICM cools, it may be experiencing thermal instability along magnetic field lines, causing it to collapse into thin, dense filaments resembling the observed H α morphology (e.g., Sharma et al. 2010). Once the cool filaments have been established, they require an ionization source to produce the high H α surface brightnesses which are observed. This heating may be due to a combination of photoionization by young stars, conduction with the hotter ICM and cosmic rays (see M+10 for a more detailed discussion).

An alternative hypothesis is that of buoyant radio bubbles (e.g., Reynolds et al. 2005, Revaz et al. 2008). In this scenario, bubbles are blown in the dense ICM by the radio-loud AGN. Due to their buoyancy these bubbles will be transported to larger radius, possibly entraining cool gas along the way. This model produces thin, radial filaments of cool gas reminiscent of the H α filaments in many cluster cores. While radio-mode feedback is likely responsible for the optical emission in a few systems (e.g., Hydra A, Abell 2052), it is hard to imagine how multiple filaments with similar surface brightnesses at a variety of orientations can be produced by this process.

5. SUMMARY AND FUTURE PROSPECTS

This study extends the work of McDonald et al. (2010) to include galaxy groups in order to determine the role of environment in the formation of H α filaments in cool cores. In summary, we find:

- The morphology and detection frequency of H α filaments in groups is similar to those seen in clusters.
- There is no obvious dependence between H α emission and the temperature of the system. There is a weak correlation between the H α emission and the mass of the system, as measured at r_{2500} . This

weak correlation may be strengthened by the inclusion of high-mass, non-cooling clusters, which are underrepresented in our sample.

- There is a weak correlation between the presence of H α filaments and the global ICM gas fraction (51% confidence level) and a strong correlation with global entropy (89% confidence level), such that H α filaments are more frequently detected in systems with low entropy and high gas fractions.
- There is a correlation between the presence of H α filaments and the properties of the cool core, namely the X-ray cooling rate (72% confidence level), the average temperature in the inner 100 kpc (55% confidence level) and the entropy at a radius of 50 kpc (84%). The correlations between the H α emission and the cooling rate and entropy in the cool core confirm previous results (Cavagnolo et al. 2008; McDonald et al. 2010) and favor the scenario where these thin filaments are the result of rapid, thermally-unstable cooling of the ICM (Sharma et al. 2010).
- The most extended H α filaments extend to the radius at which the hot ICM is cooling in ~ 3 Gyr, but not beyond. This suggests a natural timescale for the formation of filaments.
- ICM cooling is enhanced by roughly an order of magnitude in regions with H α filaments, compared to surrounding regions at the same radius.
- The cooling efficiency (cooling rate per unit gas mass) is higher in groups than in clusters, as is predicted by cooling in the absence of feedback. This is a manifestation of the weak dependence of cool cores with mass (second bullet) coupled with the strong dependence of gas content on mass. This

correlation would be further improved by the inclusion of high-mass, non-cooling clusters, which are underrepresented in our our sample.

- We confirm Sun's (2009b) finding that AGN in cool core groups have much lower radio luminosity than those in clusters. We show that this could explain the amount of feedback scaling with environment, since cool cores in groups can only survive if the amount of radio-mode feedback is small. We observe three systems with radio luminosities higher than the amount needed to remove the cool core, all of which have very disrupted cool cores and deviate from the relationship found for groups/clusters with closed feedback loops.

Our findings suggest that cool cores, and the optical line-emitting nebulae commonly associated with them, can form in groups and clusters over a large range of mass and temperature, with very little dependence on either. However, considerably larger samples will be needed to quantify whether this correlation is weak or nonexistent. We confirm the results of M+10, offering further support that the observed H α filaments in the cores of groups/clusters are intimately linked to the X-ray cooling in most systems. Without high-resolution UV imaging and optical spectroscopy, we are unable to constrain the ionization mechanism of these filaments. We plan on addressing these issues in upcoming papers.

ACKNOWLEDGEMENTS

Support for this work was provided to M.M. and S.V. by NSF through contracts AST 0606932 and AST 1009583. We thank D. Rupke, C. Reynolds, and M. Sun for useful discussions. We also thank the technical staff at Las Campanas for their support during the ground-based observations, particularly David Osip who helped in the commissioning of MMTF.

REFERENCES

- Arnaud, K. A. 1996, *Astronomical Data Analysis Software and Systems V*, 101, 17
- Blanton, E. L., Randall, S. W., Douglass, E. M., Sarazin, C. L., Clarke, T. E., & McNamara, B. R. 2009, *ApJ*, 697, L95
- Birzan, L., Rafferty, D. A., McNamara, B. R., Wise, M. W., & Nulsen, P. E. J. 2004, *ApJ*, 607, 800
- Brighenti, F., & Mathews, W. G. 2003, *ApJ*, 587, 580
- Cardelli, J. A., Clayton, G. C., & Mathis, J. S. 1989, *ApJ*, 345, 245
- Cattaneo, A., & Teyssier, R. 2007, *MNRAS*, 376, 1547
- Cavagnolo, K. W., Donahue, M., Voit, G. M., & Sun, M. 2008, *ApJ*, 683, L107
- Churazov, E., Brügggen, M., Kaiser, C. R., Böhringer, H., & Forman, W. 2001, *ApJ*, 554, 261
- Crawford, C. S., Allen, S. W., Ebeling, H., Edge, A. C., & Fabian, A. C. 1999, *MNRAS*, 306, 857
- Crawford, C. S., Sanders, J. S., & Fabian, A. C. 2005, *MNRAS*, 361, 17
- Croton, D. J., et al. 2006, *MNRAS*, 365, 11
- Donahue, M., Horner, D. J., Cavagnolo, K. W., & Voit, G. M. 2006, *ApJ*, 643, 730
- Fabian, A. C. 1994, *ARA&A*, 32, 277
- Hamuy, M., Walker, A. R., Suntzeff, N. B., Gigoux, P., Heathcote, S. R., & Phillips, M. M. 1992, *PASP*, 104, 533
- Hamuy, M., Suntzeff, N. B., Heathcote, S. R., Walker, A. R., Gigoux, P., & Phillips, M. M. 1994, *PASP*, 106, 566
- Hatch, N. A., Crawford, C. S., & Fabian, A. C. 2007, *MNRAS*, 380, 33
- Heckman, T. M., Baum, S. A., van Breugel, W. J. M., & McCarthy, P. 1989, *ApJ*, 338, 48
- Hu, E. M., Cowie, L. L., & Wang, Z. 1985, *ApJS*, 59, 447
- Jaffe, W., Bremer, M. N., & Baker, K. 2005, *MNRAS*, 360, 748
- Jones, D. H., Shoppell, P. L., & Bland-Hawthorn, J. 2002, *MNRAS*, 329, 759
- McCarthy, I. G., et al. 2010, *MNRAS*, 406, 822
- McDonald, M., & Veilleux, S. 2009, *ApJ*, 703, L172
- McDonald, M., Veilleux, S., Rupke, D. S. N., & Mushotzky, R. 2010, *ApJ*, 721, 1262
- Oke, J. B. 1990, *AJ*, 99, 1621
- Rafferty, D. A., McNamara, B. R., & Nulsen, P. E. J. 2008, *ApJ*, 687, 899
- Revaz, Y., Combes, F., & Salomé, P. 2008, *A&A*, 477, L33
- Reynolds, C. S., Casper, E. A., & Heinz, S. 2008, *ApJ*, 679, 1181
- Schlegel, D. J., Finkbeiner, D. P., & Davis, M. 1998, *ApJ*, 500, 525
- Sharma, P., Parrish, I. J., & Quataert, E. 2010, *ApJ*, 720, 652
- Sun, M., Voit, G. M., Donahue, M., Jones, C., Forman, W., & Vikhlinin, A. 2009, *ApJ*, 693, 1142
- Sun, M. 2009, *ApJ*, 704, 1586
- Veilleux, S., et al. 2010, *AJ*, 139, 145
- Vernaleo, J. C., & Reynolds, C. S. 2007, *ApJ*, 671, 171
- White, D. A., Jones, C., & Forman, W. 1997, *MNRAS*, 292, 419
- Wise, M. W., McNamara, B. R., Nulsen, P. E. J., Houck, J. C., & David, L. P. 2007, *ApJ*, 659, 1153

Name	RA	Dec	z	E(B-V)	kT
(1)	(2)	(3)	(4)	(5)	(6)
<u>Clusters</u>					
Abell 0085	00h41m50.470s	-09d18m11.26s	0.0557	0.038	5.6 ⁽¹⁾
Abell 0133	01h02m41.760s	-21d52m55.50s	0.0569	0.019	3.5 ⁽¹⁾
Abell 0478	04h13m25.274s	+10d27m54.80s	0.0881	0.517	7.1 ⁽¹⁾
Abell 0496	04h33m37.850s	-13d15m42.73s	0.0329	0.132	4.8 ⁽¹⁾
Abell 0644	08h17m25.610s	-07d30m44.94s	0.0704	0.122	6.5 ⁽¹⁾
Abell 0780	09h18m05.671s	-12d05m43.51s	0.0539	0.042	4.7 ⁽¹⁾
Abell 1644	12h57m11.608s	-17d24m33.94s	0.0475	0.069	5.1 ⁽¹⁾
Abell 1650	12h58m41.512s	-01d45m41.05s	0.0846	0.017	5.1 ⁽¹⁾
Abell 1795	13h48m52.491s	+26d35m33.85s	0.0625	0.013	5.3 ⁽¹⁾
Abell 2029	15h10m56.113s	+05d44m41.81s	0.0773	0.040	7.3 ⁽¹⁾
Abell 2052	15h16m44.501s	+07d01m18.21s	0.0345	0.037	3.4 ⁽¹⁾
Abell 2142	15h58m20.026s	+27d14m00.42s	0.0904	0.044	10.1 ⁽¹⁾
Abell 2151	16h04m35.825s	+17d43m17.81s	0.0351	0.043	3.7 ⁽¹⁾
Abell 3158	03h42m52.995s	-53d37m52.40s	0.0597	0.015	5.3 ⁽¹⁾
Abell 3376	06h02m09.717s	-39d56m59.20s	0.0597	0.056	3.5 ⁽¹⁾
Abell 4059	23h57m00.716s	-34d45m32.70s	0.0475	0.015	3.0 ⁽²⁾
Ophiuchus	17h12m27.691s	-23d22m10.41s	0.0285	0.588	8.6 ⁽¹⁾
<u>Groups</u>					
Abell 0744	09h07m20.518s	+16d39m06.70s	0.0729	0.034	2.5 ⁽³⁾
Abell 1139	10h58m11.004s	+01d36m16.49s	0.0398	0.031	2.2 ⁽³⁾
Abell 1991	14h54m31.512s	+18d38m32.57s	0.0587	0.025	2.9 ⁽³⁾
MKW4	12h04m27.082s	+01d53m45.92s	0.0200	0.017	1.8 ⁽³⁾
NGC 1132	02h52m51.830s	-02d43m30.97s	0.0231	0.055	1.1 ⁽³⁾
NGC 3402	10h50m26.093s	-13d09m17.89s	0.0153	0.039	0.8 ⁽³⁾
NGC 4325	12h23m06.665s	+10d37m16.43s	0.0257	0.023	1.0 ⁽³⁾
RBS 461	03h41m17.544s	+15d23m47.80s	0.0290	0.150	2.2 ⁽³⁾
Sersic 159-03	23h13m58.627s	-42d43m38.64s	0.0580	0.011	2.7 ⁽³⁾
UGC 842	01h18m53.621s	-02d59m52.91s	0.0452	0.040	1.8 ⁽³⁾

Table 1. – Properties of our sample of galaxy groups and clusters. X-ray temperature measurements (last column) are all from the literature – the superscript identifies the source: (1) Spatially averaged temperature (White et al. 1997), (2) Spatially averaged temperature within 100 kpc ($M+10$), and (3) Temperature at r_{2500} (Sun et al. 2009a). This sample covers a broad range in temperature, with values ranging from 1–10 keV.

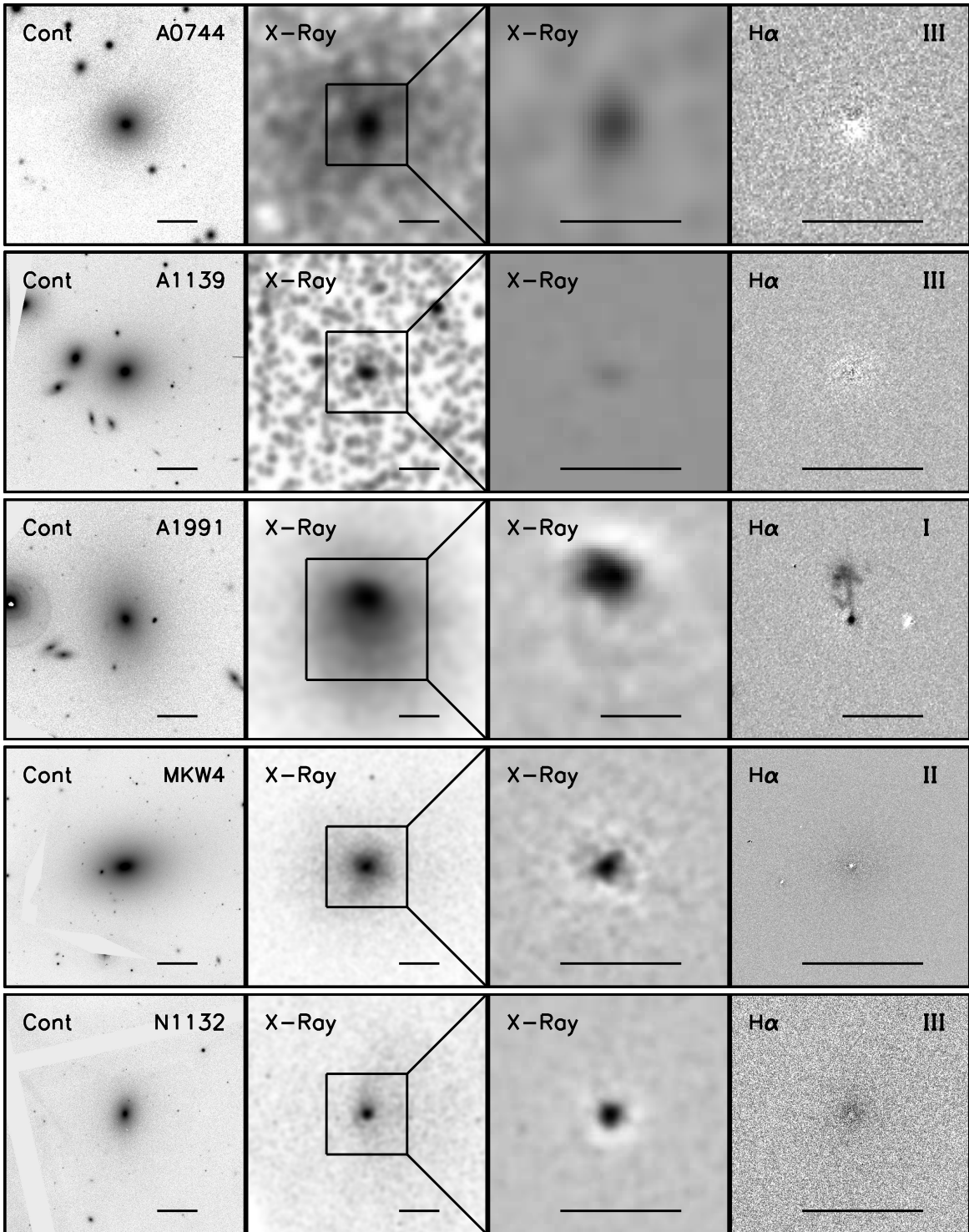


FIG. 1.— X-ray and optical data for the 10 clusters in our sample. From left to right the panels are: 1) MMTF red continuum image, 2) CXO X-ray image, 3) Unsharp masked CXO X-ray image, 4) MMTF continuum-subtracted $H\alpha$ image. The horizontal scale bar in all panels represents 20 kpc. The X-ray and red continuum images are on the same scale, and the unsharp masked and $H\alpha$ images are on the same zoomed-in scale. The square region in the X-ray panels represents the field of view for the zoomed-in panels. The grayscale in all images is arbitrarily chosen in order to enhance any morphological features.

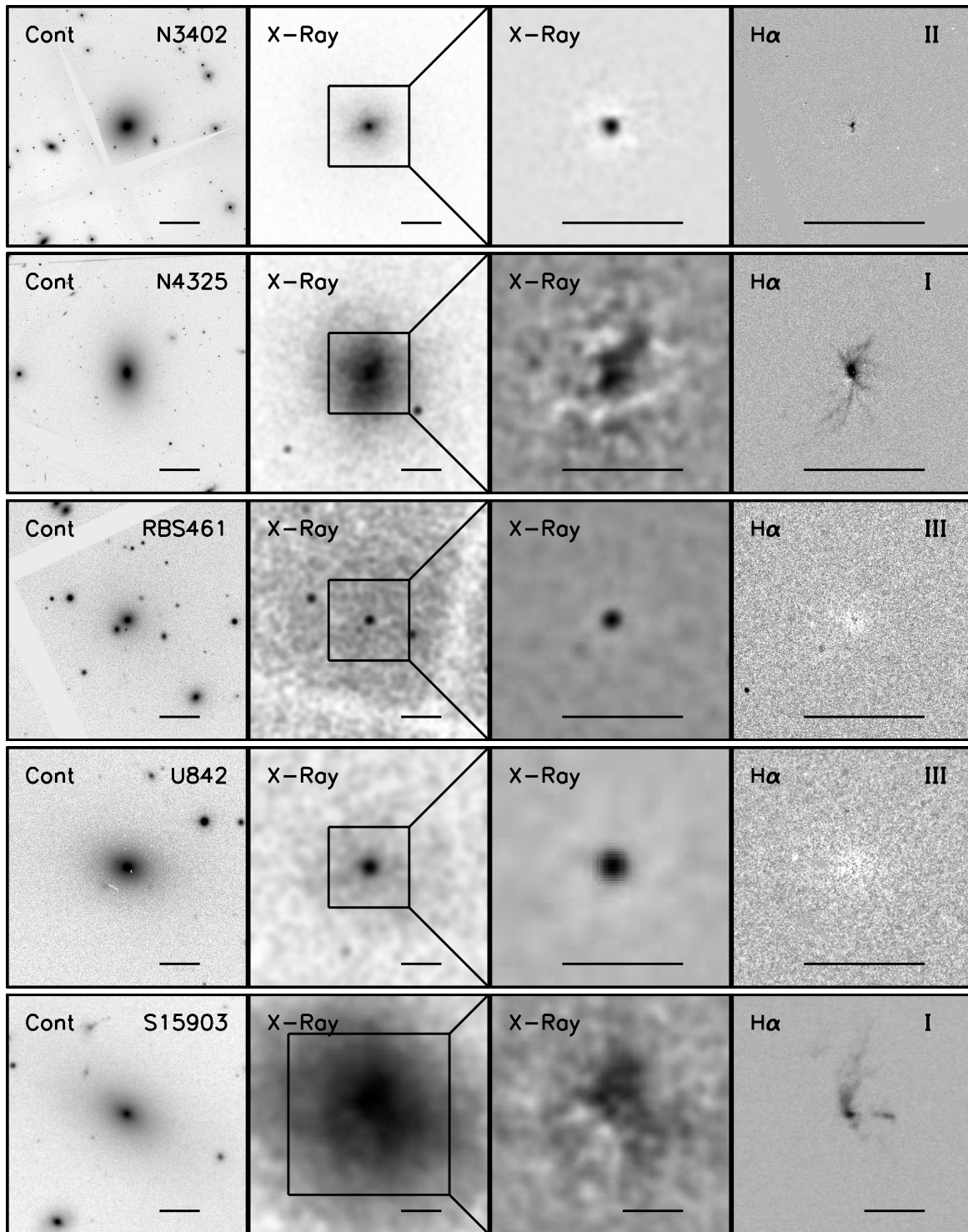


FIG. 1.— Continued.

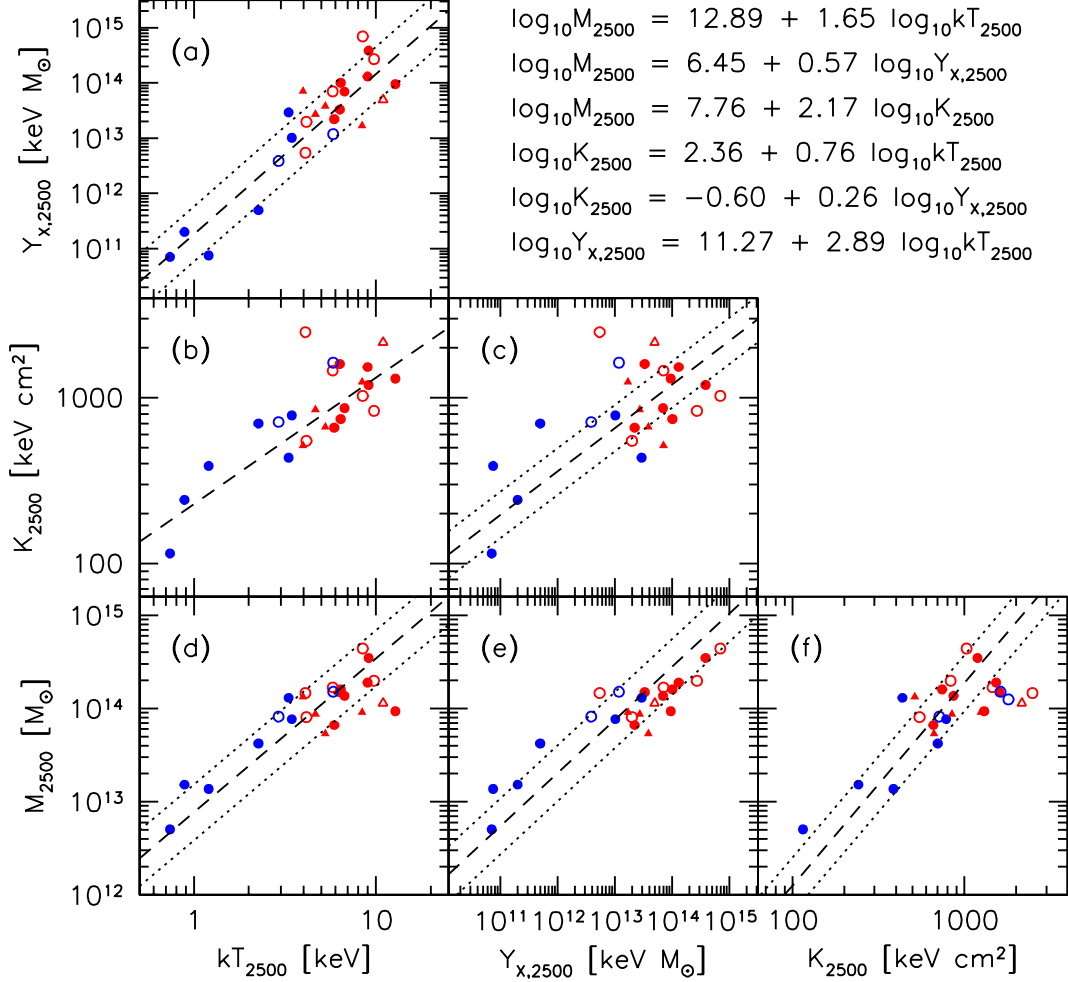


FIG. 2.— X-ray scaling relations for the 10 groups (blue) and 17 clusters (red) in our sample. The addition of groups to our sample allows us to probe the low temperature, mass and entropy regime. We differentiate between systems with $H\alpha$ emission (filled circles) and those without (open circles). Systems that are clearly disturbed either by mergers or AGN feedback are depicted by triangles and typically have under-estimated M_{2500} . The high-temperature, undisturbed outlier in panel (d) is Ophiuchus, which lies in the Galactic plane and, thus, suffers from heavy extinction. The high-entropy outlier in panels (b), (c) and (f) is Abell 2151, which requires the largest extrapolation from the last data point to r_{2500} , and thus has the least constrained properties. For comparison, we show relations derived from Sun et al. 2009a for several of the same systems (dashed lines). We show the functional form of these relations in the upper right corner. The scatter in these relations (dotted lines) represents our uncertainty in converting quantities from r_{500} to r_{2500} . For panel (b), we plot the exact relation quoted by Sun et al. 2009a.

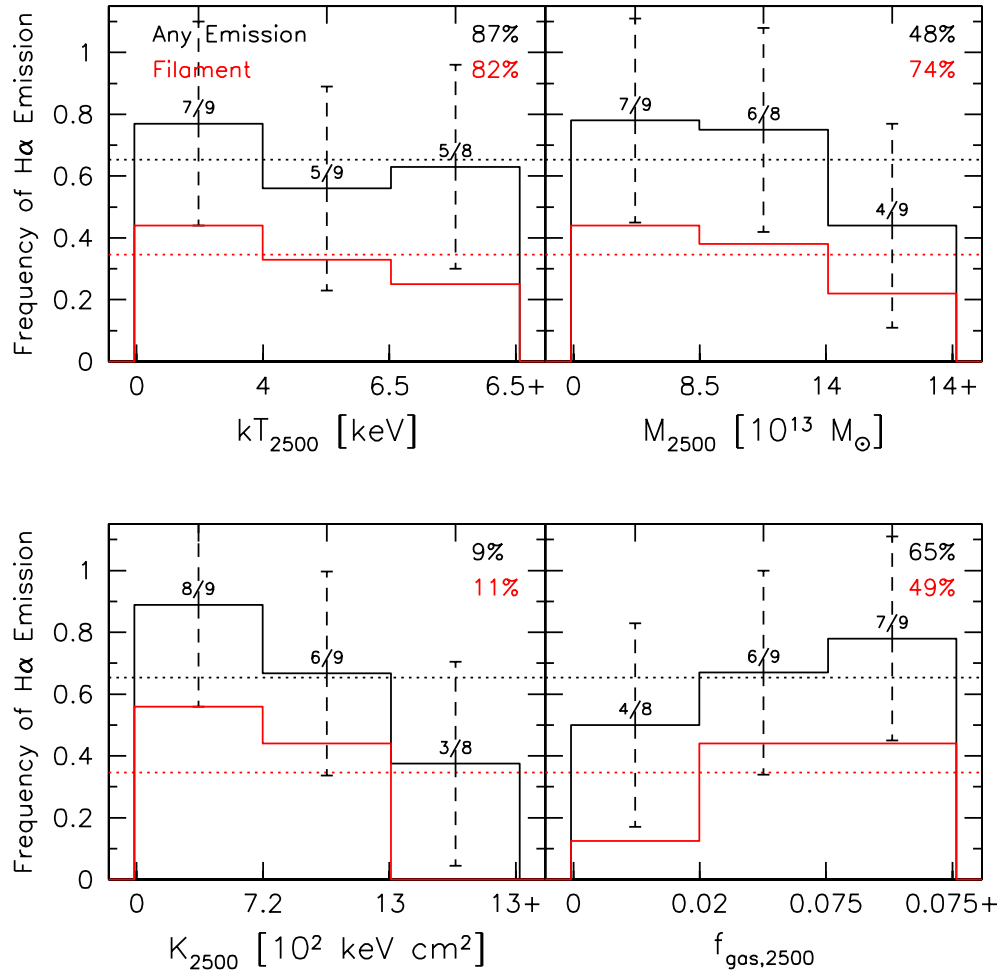


FIG. 3.— Frequency with which we observe H α emission in clusters and groups, as a function of the global X-ray properties. The black histograms show the frequency with which we detect any H α emission whatsoever, while the red histograms show the frequency with which we detect extended H α filaments. The horizontal lines represent the overall detection rate, while the vertical errorbars represent the 1- σ uncertainty in a given bin. The absolute number of systems in each bin are shown above the black histograms. We find that there is no measurable correlation between the global temperature and the presence of H α emission. There is a weak correlation between the presence of H α and the global mass, and stronger correlations with both entropy and gas mass fraction, however these are at the $< 1\text{-}\sigma$ level. The black and red numbers represent the F-test confidence with which we can reject the hypothesis of a steadily rising/falling distribution in favor of a flat distribution, for all H α emission and emission in filaments, respectively.

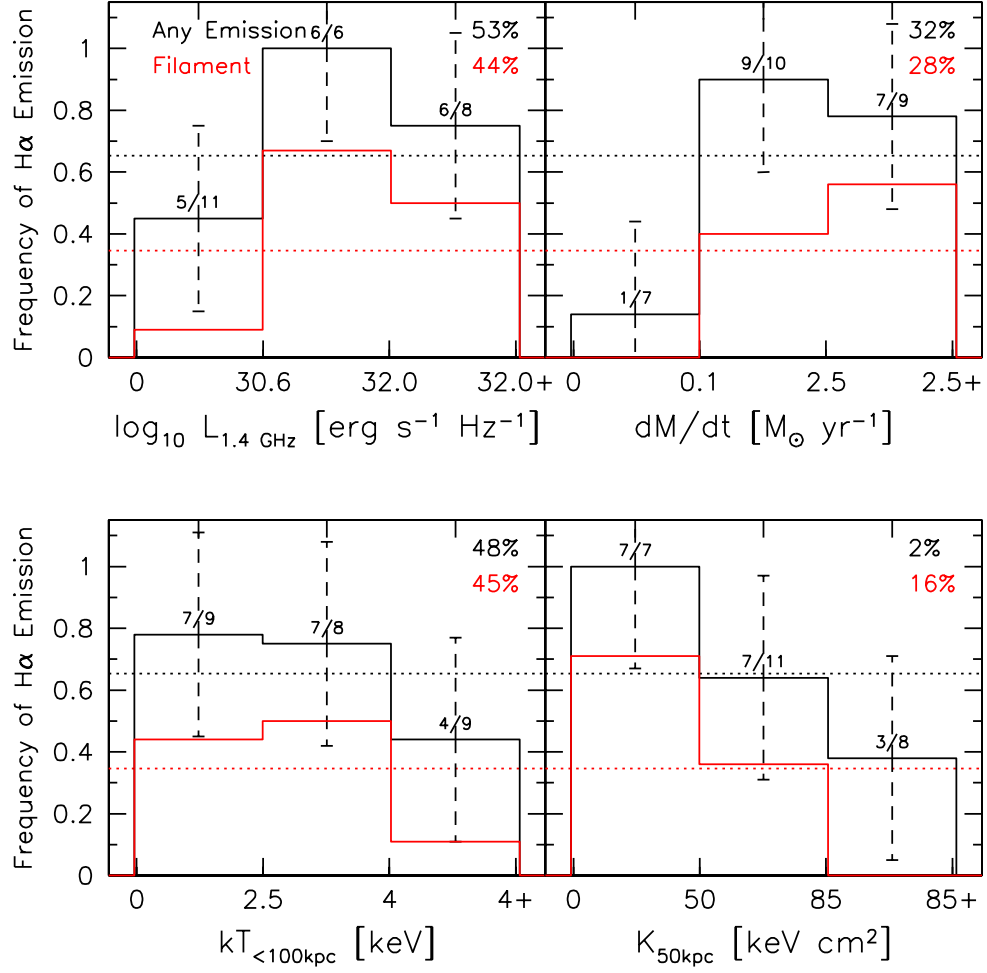


FIG. 4.— Frequency with which we observe H α emission in clusters and groups, as a function of the X-ray properties in the group/cluster core. The black histograms show the frequency with which we detect any H α emission whatsoever, while the red histograms show the frequency with which we detect extended H α filaments. The horizontal lines represent the overall detection rate, while the vertical errorbars represent the $1-\sigma$ uncertainty in a given bin. The absolute number of systems in each bin are shown above the black histograms. We find that the correlation between H α and 1.4 GHz flux to be slightly weaker than between the H α flux and the X-ray cooling rate. We also see anti-correlations between the presence of H α emission and the core temperature and entropy, as reported in M+10. The black and red numbers represent the F-test confidence with which we can reject the hypothesis of a steadily rising/falling distribution in favor of a flat distribution, for all H α emission and emission in filaments, respectively.

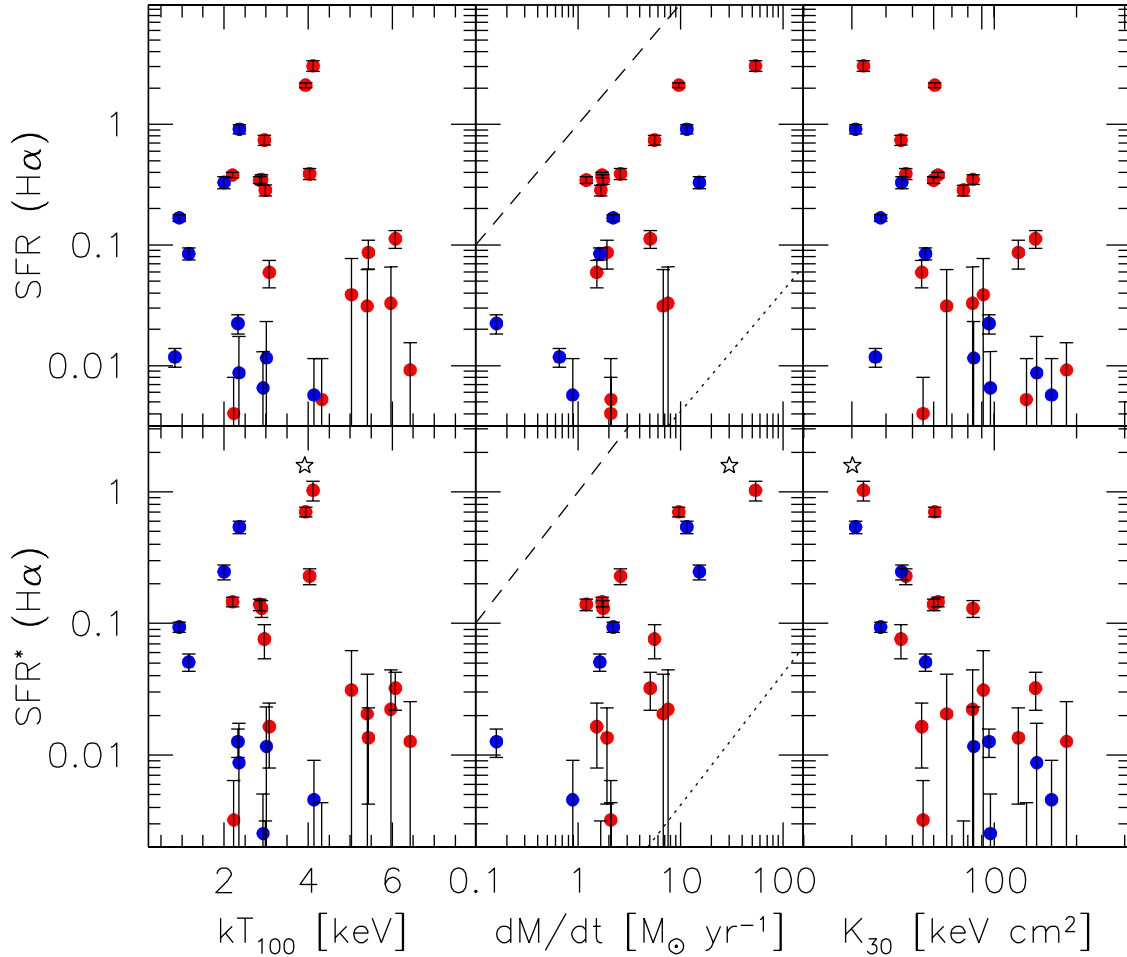


FIG. 5.— $H\alpha$ luminosity, quoted as a star formation rate based on Kennicutt (1998), plotted against the average temperature in the inner 100 kpc (kT_{100}), specific entropy at 30 kpc (K_{30}), and the integrated mass deposition rate (dM/dt). Red points in this plot represent clusters from M+10, while the blue points refer to the groups sample in this paper. The SFRs in the lower panels have had the nuclear contribution removed (SFR*). The open star in the lower panels refers to Perseus A (Conselice et al. 2001, Sanders et al. 2004). The diagonal dashed line represents the limit where all of the cooling X-ray gas turns into stars, while the dotted line is the case where all of the cooling X-ray gas is made up of hydrogen which recombines only once (Fabian et al. 1984).

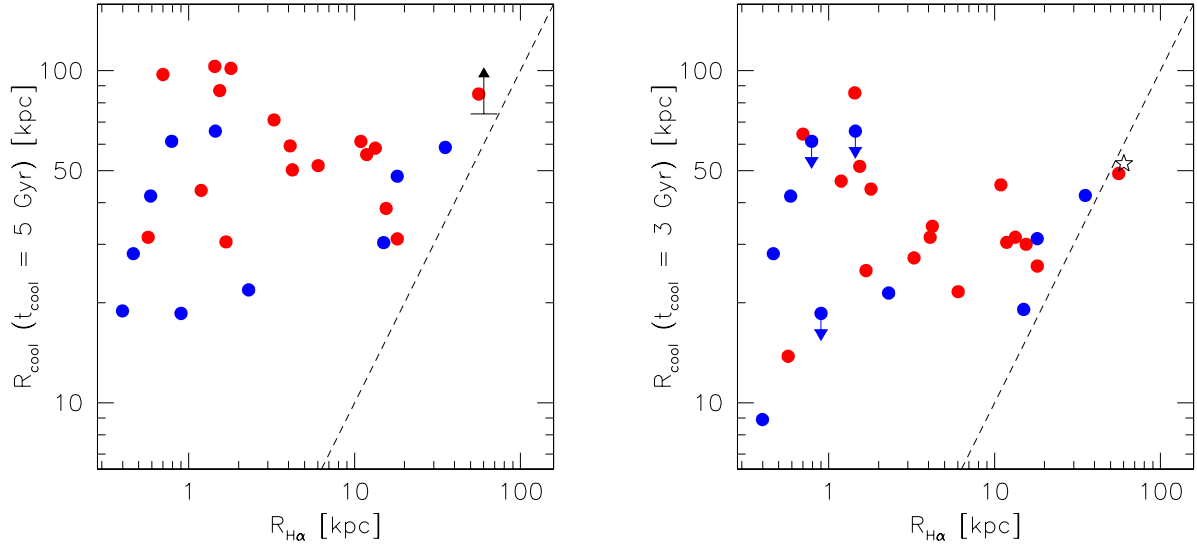


FIG. 6.— Left: Correlation of R_{cool} , the radius at which the cooling time of the ICM reaches 5Gyr; and $R_{H\alpha}$, the largest radius at which we detect $H\alpha$ emission. When there was no detected $H\alpha$ emission an upper limit of the seeing FWHM has been enforced. The dashed line refers to the one-to-one case, while the point colors refer to the clusters from M+10 (red) and the groups from this paper (blue). There appears to be an upper limit on the radius of $H\alpha$ filaments, corresponding to the cooling radius. The black point represents a lower limit estimate on the cooling radius of Perseus A (Fabian et al. 2000, Conselice et al. 2001). Right: Similar to plot on the left, but using a cooling time of 3Gyr to define the cooling radius. Perseus, Abell 1795, and Sersic 159-03 lie almost exactly on the 1-to-1 line in this case.

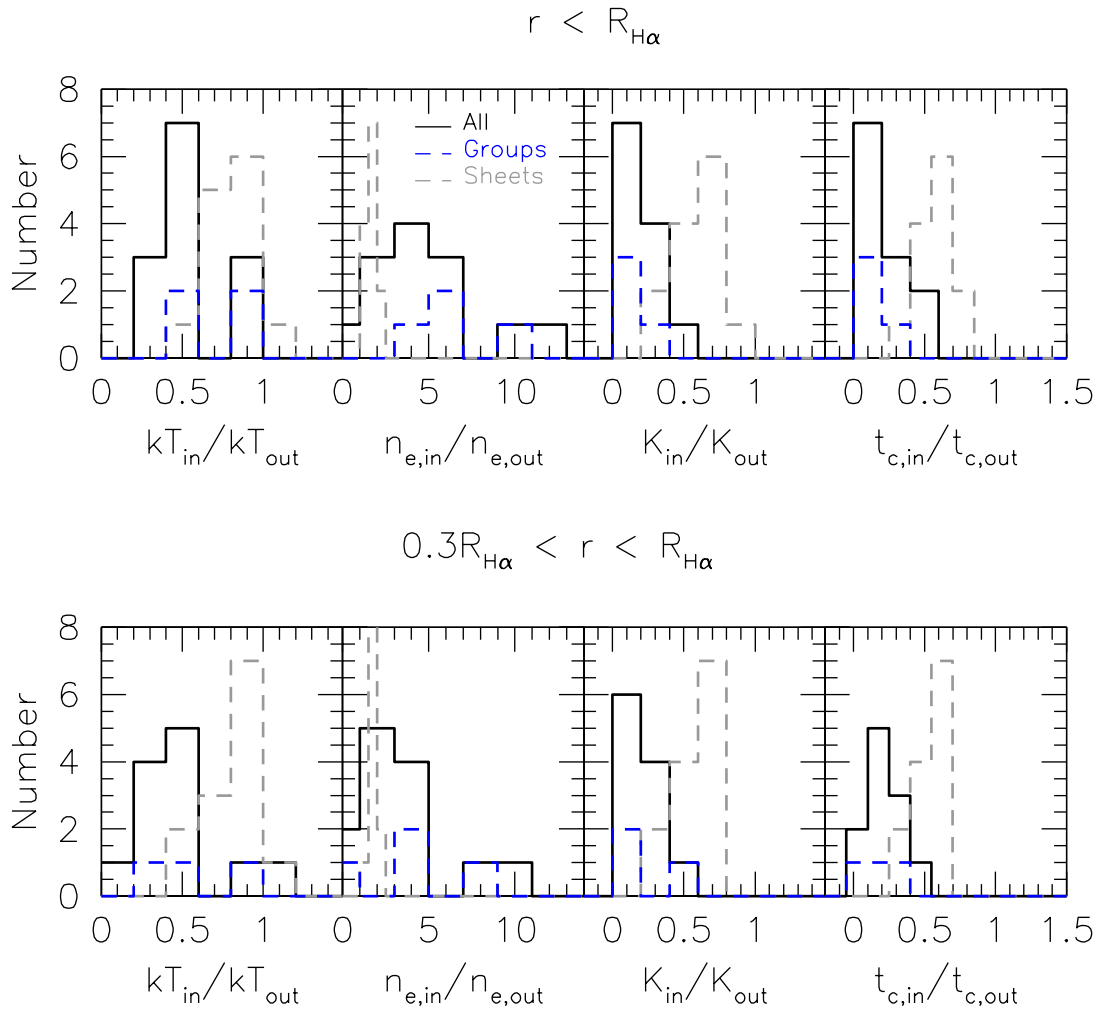


FIG. 7.— Upper panels: Distribution of temperature, electron density, entropy, and cooling time ratios in and out of the $H\alpha$ filaments. The solid black and dashed grey lines bracket the extreme cases of the filament geometry: solid black lines are the thin-filament case, which is modeled with a two-temperature plasma, while the grey dashed lines are the case of single-temperature sheets of gas seen edge-on. The blue, dashed lines show the contribution to the total histogram from galaxy groups. The in-filament gas shares similar properties with the cool core, namely that the X-ray gas has a cooling time of $\sim 10\%$ that of the surrounding ICM. There appears to be no difference in the properties of the filaments in groups and clusters. Lower panels: Similar to the above panels, but now considering only the outer 70% of the filaments in radius, in order to remove the contribution from the central, circularly symmetric, region.

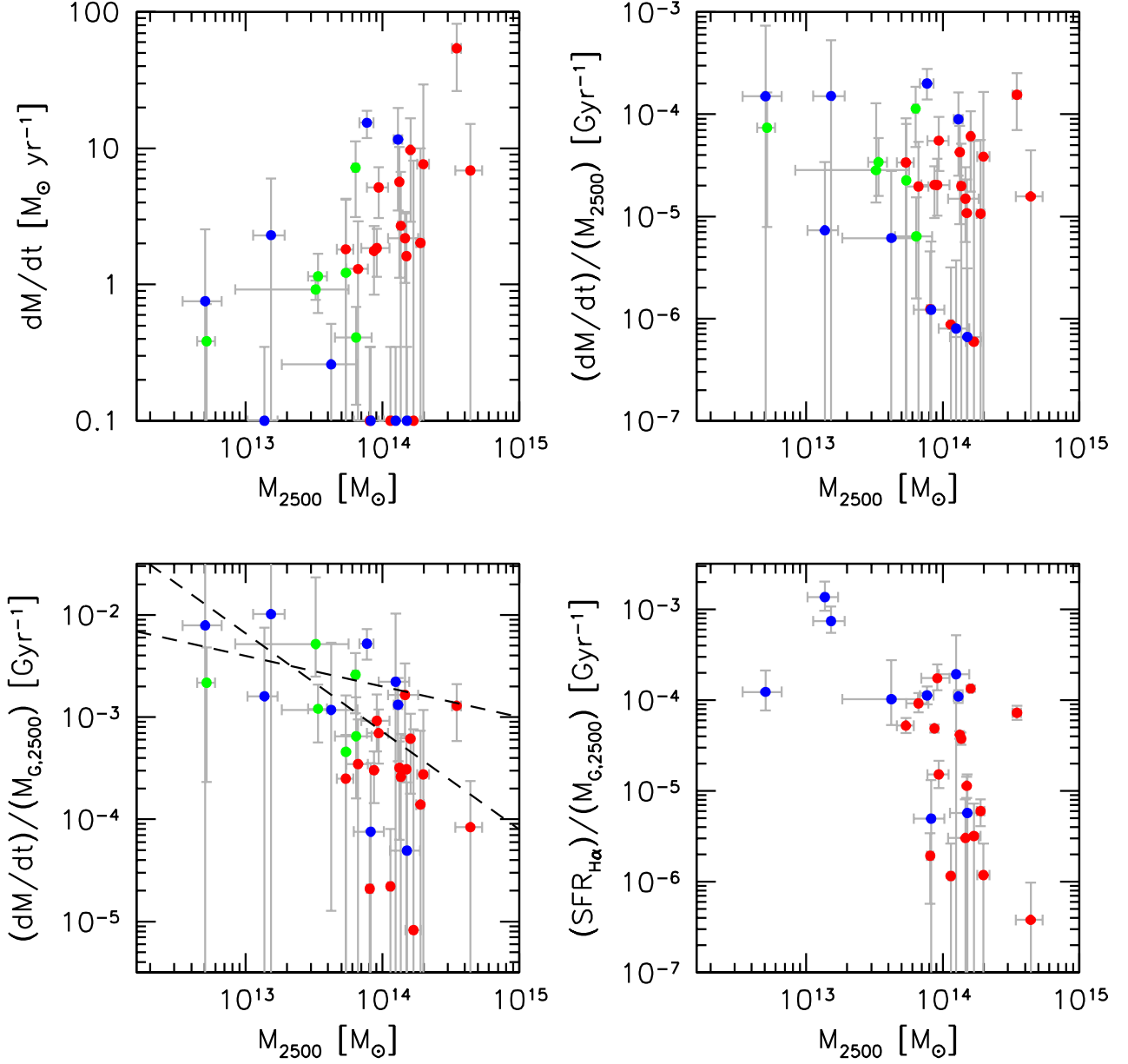


FIG. 8.— Upper left: X-ray cooling rate (dM/dt) as a function of M_{2500} , the mass enclosed within r_{2500} . Red and blue points refer to the cluster and group samples, respectively. Green points are six new groups taken from the Sun et al. (2009a) sample in order to better sample the X-ray properties of the groups. Upper right: X-ray cooling rate per unit total mass as a function of M_{2500} . We note an apparent upper limit on this scaled cooling rate at $\sim 2 \times 10^{-4} \text{ Gyr}^{-1}$. Lower left: ICM cooling efficiency (cool rate per unit gas mass) as a function of M_{2500} . The dashed lines reflect the expected slopes for Bremsstrahlung (-0.3) and line cooling (-0.96). The zeropoints for these lines were adjusted to best fit the data. The fact that the data matches the general predicted trend suggests that the effect of feedback must either be negligible or scale with total mass, otherwise the trend would be altered. Lower right: $H\alpha$ -determined star formation rate per unit gas mass versus M_{2500} . Similar trends are noted here since $L_{H\alpha}$ is an excellent proxy for dM/dt (M+10).

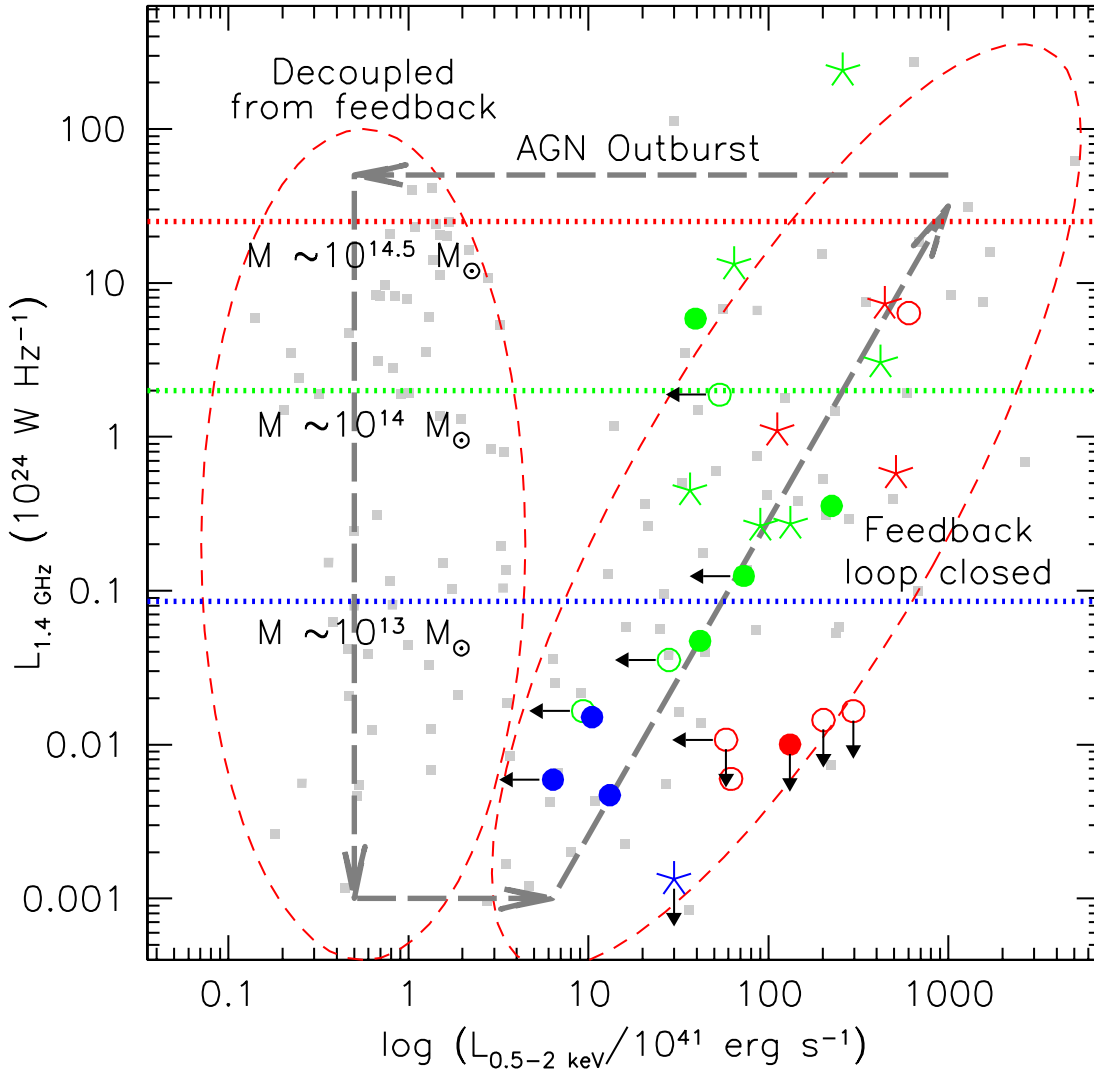


FIG. 9.— 1.4 GHz radio luminosity versus integrated soft X-ray luminosity within the cooling radius. Color refers to the system mass, with blue, green and red referring to systems with $M_{2500} \sim 10^{13} M_{\odot}$, $10^{14} M_{\odot}$, and $10^{14.5} M_{\odot}$, respectively. Stars, closed circles and open circles are systems with filamentary, nuclear or no $H\alpha$ emission. Grey points are groups and clusters from Sun (2009b) and the red ellipses describe the two loci identified by Sun. The grey arrows show the proposed evolution of systems from cool, feedback-regulated cores (right ellipse) to X-ray faint corona (left ellipse). If the radio luminosity exceeds a certain threshold, depicted by horizontal dotted lines, the amount of feedback exceeds the required $p dV$ work needed to disrupt the cool core. This simple picture seems to have some merit, as the three clusters in our sample with extremely disrupted cores (Hydra A, Abell 2052, Abell 4059) all have radio luminosities exceeding the allowable threshold for their mass and are significantly offset to the left of the cool core locus. This plot provides an explanation for the fact that groups with cool cores tend to have low-luminosity AGN when compared to their high-mass counterparts.